Microstructure assessment of suspension plasma spraying coatings from multicomponent submicronic Y-TZP/Al_2O_3/SiC particles

Víctor Carnicer[1*], Mª José Orts[1], Rodrigo Moreno[2], Enrique Sánchez[1]

(1) Instituto de Tecnología Cerámica (ITC), Universitat Jaume I (UJI). Castellón, Spain

(2) Instituto Cerámica y Vidrio (ICV), Consejo Superior de Investigaciones Científicas (CSIC). Madrid, Spain

Víctor Carnicer (*corresponding author)

Telephone number: +34 964 342424 Fax number: +34 964 342425

Email: victor.carnicer@itc.uji.es

Postal address: Instituto de Tecnología Cerámica (ITC). Campus Universitario Riu Sec. Av. Vicent Sos Baynat s/n 12006 Castellón (Spain)

Abstract

In this research, Suspension Plasma Spraying (SPS) technique was used for the thermal deposition of a multicomponent mixture made up of an Y-TZP/Al_2O_3 matrix with SiC particles. Two suspensions of Y-TZP and Al_2O_3 with different SiC particle content (6 wt% and 12 wt%) were tested as feedstocks in the SPS process. Three stand-off distances were varied in order to assess coating microstructure and quantify SiC particles preservation in the final coatings. Coatings were characterised in terms of porosity, microstructure and phase distribution. The estimate of the amount of SiC particles present in the coating was carried out by XRD technique.

Findings showed typical cauliflower-like SPS microstructure which intensifies with stand-off distance. Coatings porosity values varied significantly between 8 to 25% whereas minimum porosity was found for the intermedium stand-off distance of 40 mm.

Microstructure analysis also revealed the presence of SiC particles in the coatings which was confirmed by EDX analysis, overall XRD test as well as TG analysis compared with SiC powder. Finally, quantification of SiC content in the final coatings by means of XRD analysis showed that most of SiC particles (c.a 80 %) of the feedstocks were preserved in the final coatings.

Key words: SPS process, SiC deposition, TBCs, self-healing coatings

1. Introduction

The most widely used material of thermal barrier coatings (TBCs) is currently yttria-stabilised zirconia (YSZ) due to its low thermal conductivity, relatively low coefficient of thermal expansion, phase stability and high corrosion resistance [1]. The state-of-the-art TBC system consists of a bilayer coating made up of a thermally insulating yttria-stabilized zirconia YSZ top coat applied over an oxidation-resistant MCrAlY (M = Ni

and/or Co) bond coat [2]. With regard to processing, atmospheric plasma spraying (APS) is one of the most common techniques to produce these coatings due to its good balance between coating performance and low cost [3]. In the last years Suspension Plasma Spraying (SPS), a more recent technique in thermal spraying field in which particle suspensions are used as feedstocks, is attracting great interest in the scientific community to obtain TBCs due to the possibility of directly feeding very fine particles into the plasma torch leading to enhanced coating microstructure for TBC performance [1,4–6].

However, YSZ displays a crystalline-phase change at long lifetimes or at very high temperatures (>1200 °C) which causes a damage or failure of the TBC. This latter, along with the growing need in the last years for increasing the operational temperature of gas turbines has fuelled an intense research activity to develop coatings systems with enhanced thermal isolation and performance [7–9]. These advanced TBC coatings requirements have also led to the seek of new TBC materials, the development of new coating architecture for the existing materials or a combination of both approaches. Thus, new materials stable at higher temperatures and with lower thermal conductivity than YSZ, multilayer systems with different functions or graded structures or compositions are now under intense research activity [10–14]. More recently, several research groups have proposed to develop a new generation of TBCs with self-healing ability, which is expected to contribute to enhance working conditions of the turbines and prolong their lifetime [15–17]. SiC is reported as the most efficient ceramic self-healing material, although other metals and alloys are being also investigated [18–20]. Nevertheless, in the case of SiC, the coating process should guarantee as much as possible the preservation of the sealing agent particles present in the starting feedstock once SiC particles have travelled through the plasma torch and have been deposited on the substrate.

In a previous paper the authors reported a first part of a research based on a mixed strategy which has been chosen to avoid the oxidation of SiC (self-healing agent) during plasma deposition [21]. Firstly, SPS technique was used for the thermal deposition trying to minimise the exposition of SiC particles with an excessively energetic plasma plume by feeding an aqueous suspension instead of a solid particles mixture. Secondly, a third component (Al_2O_3) was added to the Y-TZP matrix in order to contribute to protect SiC particles against oxidation during plasma deposition by means of the formation of an eutectic mixture [22]. The research showed that optimal suspension feedstock containing SiC particles was successfully deposited by SPS. In this second part of the research spraying conditions (stand-off distance) will be varied in order to assess coating microstructure and more importantly, quantify SiC particles preservation in the final coating. Two suspensions of Y-TZP and Al_2O_3 with different SiC particle content will be used as feedstocks in the SPS process. Coatings will be characterised in terms of porosity, microstructure and phase distribution. The estimate of the amount of SiC particles present in the coating will be carried out by XRD technique.

2. Experimental procedure

2.1. Feedstock preparation and characterisation

As starting raw materials, the following commercially available powders were used: α-alumina (CT3000SG, Almatis, Germany), tetragonal zirconia polycrystals doped with 3 mol% Y_2O_3 (TZ-3YS, Tosoh, Japan) and α-SiC (UF-15, Hermann C. Starck, Germany). The two oxides were mixed together in such concentrations as to produce after sintering the eutectic composition, i.e. with a relative zirconia/alumina weight ratio of 59.6/40.4.

Some characteristics of these three powders are shown in Table 1. Further details on these materials can be consulted in previous work [21].

Table 1 Some characteristics of commercial powders employed in this research.

Characteristics	Y-TZP	Al_2O_3	SiC
Particle size / D_{50} (µm)	0.4	0.5	0.6
Main crystalline phases	t/m 68/32*	α	α
Specific surface area (m^2)	6.8	8.0	15.0
Density (g/cm^3)	6.05	3.97	3.21

* t/m: tetragonal/monoclinic ratio obtained from Garvie's approach [23].

Feedstock suspensions containing 10 vol.% solids were obtained as follows. Firstly, mixtures of the two oxides were prepared using a two-step process in which zirconia was added to the total water containing the deflocculant required for its dispersion and in a second step the alumina powder was incorporated after adding the deflocculant required for its dispersion. In both cases the deflocculant used was ammonium salt of polyacrylic acid (PAA; Duramax TM D-3005, Rohm & Haas, USA, with 35 wt% active matter) as reported elsewhere [24]. The deflocculant content was 0.2 wt% PAA for both oxides. Secondly, suspensions with SiC were prepared following this sequence with the final addition of SiC after the incorporation of 1.5 wt% of the deflocculant PKV (Produkt KV5088, Zschimmer-Schwarz, Germany) [25]. The contents of SiC in the final formulation were 6 wt% and 12 wt%. The required amount of the used deflocculants for the preparation of each component of the feedstock suspension has been reported in the previous research [21]. The rheological behaviour of these two suspension feedstocks was determined using a rheometer (Haake RS50; Thermo, Karlsruhe, Germany) operating at controlled shear rate by loading the shear rate from 0 to 1000 s^{-1} in 5 min, maintaining at 1000 s^{-1} for 1 min and uploading from 1000 to 0 s^{-1} in 5 min. The measurements were

performed at 25°C using a double-cone and plate system with a cone angle of 2°, equipped with a solvent trap to avoid evaporation.

Sedimentation tests, to determine the stability of the suspensions were carried out by multiple light scattering (Turbiscan^{TM} LAB Stability Analyzer, Formulaction, France), which can measure the variation with time of the amount of light backscattered by the suspended solids and the percentage of light transmitted by the liquid along the glass cell that contains the suspension. As a result, a family of curves (each one corresponding to a measurement of time) is obtained, which represents the percentage of light backscattered or transmitted as a function of glass cell height [26]. Sedimentation measurements were carried out from 1 h to 72 h.

2.2. Coating deposition

Both suspension feedstocks (6 wt% and 12 wt% SiC) were sprayed on metallic substrates by an SPS system. This system, developed by the Institute for Ceramic Technology (ITC, Castellón, Spain), is formed by two pressurised containers which force the liquid to flow through a 150 μm diameter injector [27]. A filter was used to remove agglomerates larger than 75 μm and possible contaminations. Coatings were deposited with a plasma torch (F4-MB, Sulzer Metco, Switzerland) managed by a six axes robot (IRB 1400, ABB, Switzerland) employing argon as primary plasma gas and hydrogen as secondary plasma gas. The substrates, which were made of AISI type 304 stainless steel, had disc shape with a diameter of 25 mm. Prior to coatings deposition, substrates were grit-blasted using black corundum until a surface roughness (R_a) of 2.2 ± 0.1 μm was reached and then cleaned with ethanol. A commercial bond coat (Amdry 997) was previously deposited on the metallic substrate by atmospheric plasma spraying (APS) as set out elsewhere [28]. This bond coat powder had a particle size distribution ranging from 5 to 38 μm and a composition (in wt%): 43.9 Ni, 8.5 Al, 23 Co, 20 Cr, 4 Ta, 0.6 Y. Finally, metallic

substrates were preheated at 300°C to further improve the adhesion of the coating during deposition.

The following spraying parameters to deposit the top coat were kept constant from previous optimisation task: 37 slpm Ar, 8 slpm H_2, 700 A intensity, 1.25 m/s spraying velocity, 27 ml/min suspension feed rate and 0.72 m/s specimen holder velocity. In order to vary the plasma energy three stand-off distances were tested: 30 mm, 40 mm and 50 mm. Five torch scans were carried out for all the spraying experiments in order to obtain similar thickness in the final coatings.

2.3. Coating characterisation

The coatings microstructure was analysed on as-sprayed surfaces as well as on polished cross-sections using a field-emission scanning electron microscope (Quanta 200FEG, FEI Company, USA). The crystalline phases of the different coatings were identified by X-ray diffraction (XRD) with an Advance Diffractometer, Bruker Theta-Theta, Germany. The analysis was carried out with powder samples, Cu kα radiation (λ= 1.54183 ˚A), energy settings of 40 kv and 40 mA, 2θ range between 5 - 90˚, and a scanning speed and step size of 10 s and 0.02˚ (2θ) respectively. Subsequently, for the quantification of the silicon carbide content in the coatings, the test was carried out on the same powder samples using Cu kα radiation (λ= 1.54183 Å), energy settings of 40 kv and 40 mA, a limited range in 2θ of 33 - 36.5˚ and a scanning speed and step size of 10s and 0.01˚ (2θ). Thus, intensities of the SiC d= 2.516Å diffraction peak (PDF 04-010-5698) were compared on powder samples of the feedstocks before and after being introduced into the plasma torch. Assuming that there is no significant change in the global composition of the powder during plasma deposition (evaporation is not relevant), the mass absorption coefficient of both samples is constant and as peak intensity is directly proportional to

the SiC content, the SiC peak intensity ratio coincides with the ratio of SiC concentration in the powder before and after passing the plasma torch [29].

Coatings thickness and porosity were estimated by image analysis (MicroImage) at 2000x magnifications from SEM pictures following a procedure set out elsewhere [21]. For each sample, 20 SEM images were examined and the findings averaged. TG-DTG tests were carried out on the same powder samples collected once the suspension feedstocks got through the plasma torch with the aim at further assessment of SiC presence in the final coatings. These tests were performed in a Mettler TGA/STDA 815e thermobalance at a heating rate of 10 °C·min^{-1} at a maximum tested temperature of 1200 °C.

3. Results and discussion

3.1. Feedstock characterisation

Fig. 1 shows the flow curves of both suspension feedstocks (6 wt% and 12 wt% SiC) prepared at a solids content of 10 vol.% (~35 wt%). For comparison purposes the curve of the alumina/zirconia composition without SiC particles at the same solid concentration is also included (0 wt%). In this same figure, viscosity versus shear rate curves are also displayed. As it can be observed, addition of SiC particles has not any influence on suspension rheology that maintains always Newtonian. In fact, the viscosity is extremely low, of very few mPa.s, which is in the minimum range that can be measured with a rotational rheometer. This makes the curves to present an apparent shear thickening as a consequence of wall slippage that is typically observed in sol-gel solutions, which are known to be Newtonian. As the shear rate inside the injector is very high (> 1000 s^{-1}) because of the very small nozzle diameter, the viscosity at the maximum measured shear rate (1000 s^{-1}) was determined to be 3.3 mPa.s for all three slurries. The extremely low viscosity values at any shear rate allows the suspensions to be stored and fed into the

plasma torch through the peristaltic pumping without any problem. As also observed in Fig. 1 thixotropy values which are related to as the area enclosed in the hysteresis loop in flow curves are negligible. Therefore, suspension rheological behaviour is expected to keep practically invariable after rest time or agitation for long time [30].

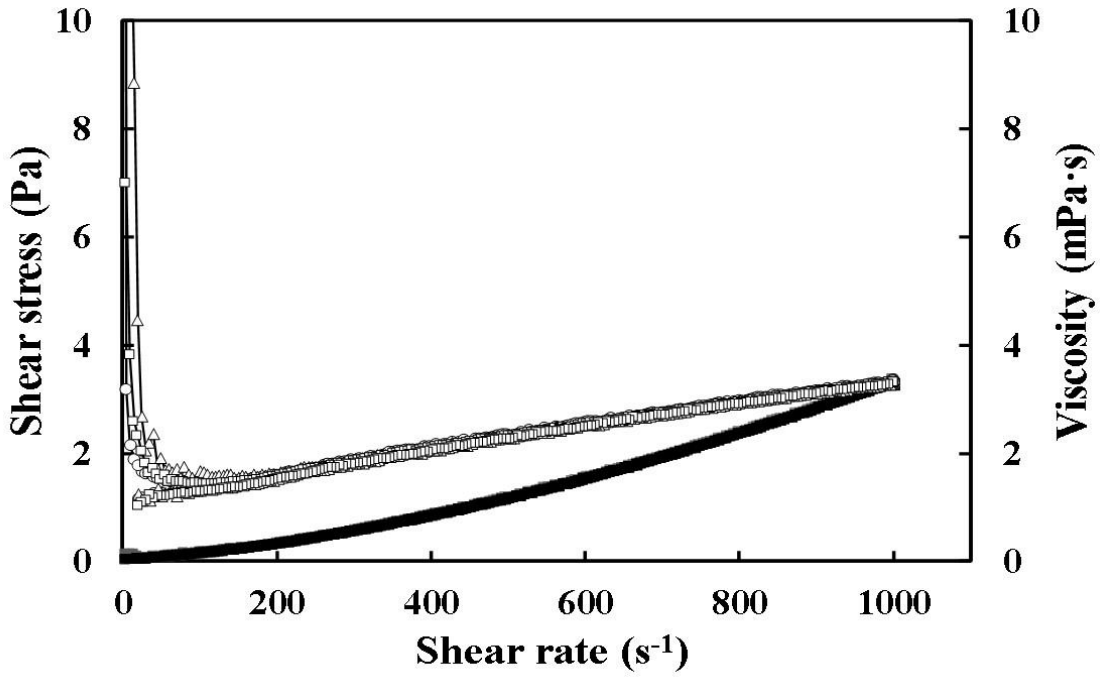

Fig. 1 Flow and viscosity curves for 6 wt% SiC feedstock and 12 wt% SiC feedstock. For comparison, the curves of the alumina/zirconia suspension without SiC particles (0 wt%) are also included (□ 0 wt%, △ 6 wt% and ○ 12 wt% (open symbols for shear stress plot and bold symbols for viscosity plot).

Otherwise, Fig. 2 sets out the results of the sedimentation tests. As previously reported, sedimentation tests in a multiple light scattering equipment allow to determine the stability of the suspensions [31]. As a result of the test, a few curves are obtained, each one representing the percentage of light backscattered or transmitted as a function of glass cell height at a given time. Thus, for 1 h the suspension is quite stable, since no sedimentation occurs as Fig. 2 shows. But, over 5 h sedimentation starts to be appreciable, since the curve profile departs from that of the starting suspension at high cell heights

[26]. At longer times increasing sedimentation occurs. Nevertheless, as the suspension is easily redispersable, it would be enough to agitate this sediment (or longer time stay sediments) to obtain again a stable suspension for 5 h more. On the other hand, both sets of curves display similar evolution with time what indicates that SiC particle content do not affect suspension stability. This time of stability of 5 h can be considered sufficient for the SPS process. In fact, the estimated time that the suspension stays in the SPS container and circuit for a real sample could be lower than 1 hour, depending on the type and dimensions of the sample to be obtained.

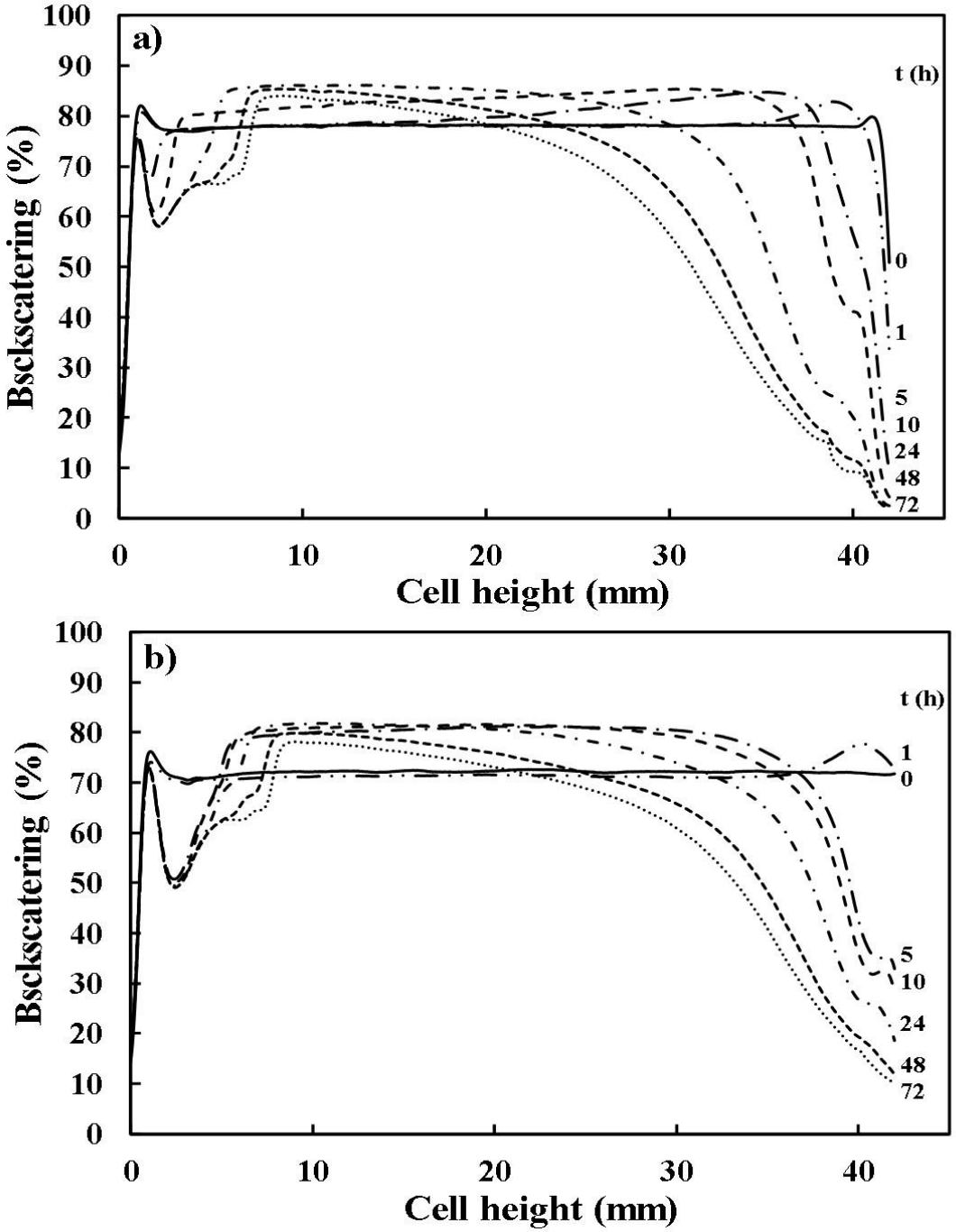

Fig. 2 Sedimentation curves for a) 6 wt% SiC feedstock and b) 12 wt% SiC feedstock at different sedimentation times (in hours), indicated on the right side of the figures.

3.2. Coating microstructure

Fig. 3 shows the surface micrographs of the surface coatings obtained from the two suspension feedstocks (6 wt% and 12 wt% SiC) at the three stand-off distances (30, 40 and 50 mm). These micrographs reveal the typical surface microstructure adopted by SPS coatings as reported elsewhere [32,33]. In SPS process the suspension is injected into the plasma jet and the liquid evaporates. The remaining fine solids can melt and agglomerate with other molten particles or can remain as solid particles, depending on their trajectory in the plasma jet. Cauliflower-like microstructure (from surface view) or columnar-like microstructure (from cross-sectional view) are described in the literature [33] as typical microstructures for different suspension feedstocks regardless the nature or solid concentration of SPS suspension. Sokolowski et al. [33] have modelled these microstructures, which relate to a force balance onto the rough substrate surface. Basically, the SPS technique, due to the lower in-flight velocity of the particles and agglomerates (in comparison with powder feedstocks in APS process) always produces more porous, rougher layers with columnar-like growth. This cauliflower-like structure is clearly observed in the surface micrographs of Fig. 3. In addition, independently of the amount of SiC particles, the cauliflower-like microstructure becomes more pronounced as the stand-off distance increases as a consequence of the re-solidification phenomenon associated with longer distance run by the molten particles or agglomerates [24,34]. This is particularly visible when stand-off distance grows from 30 to 40 mm.

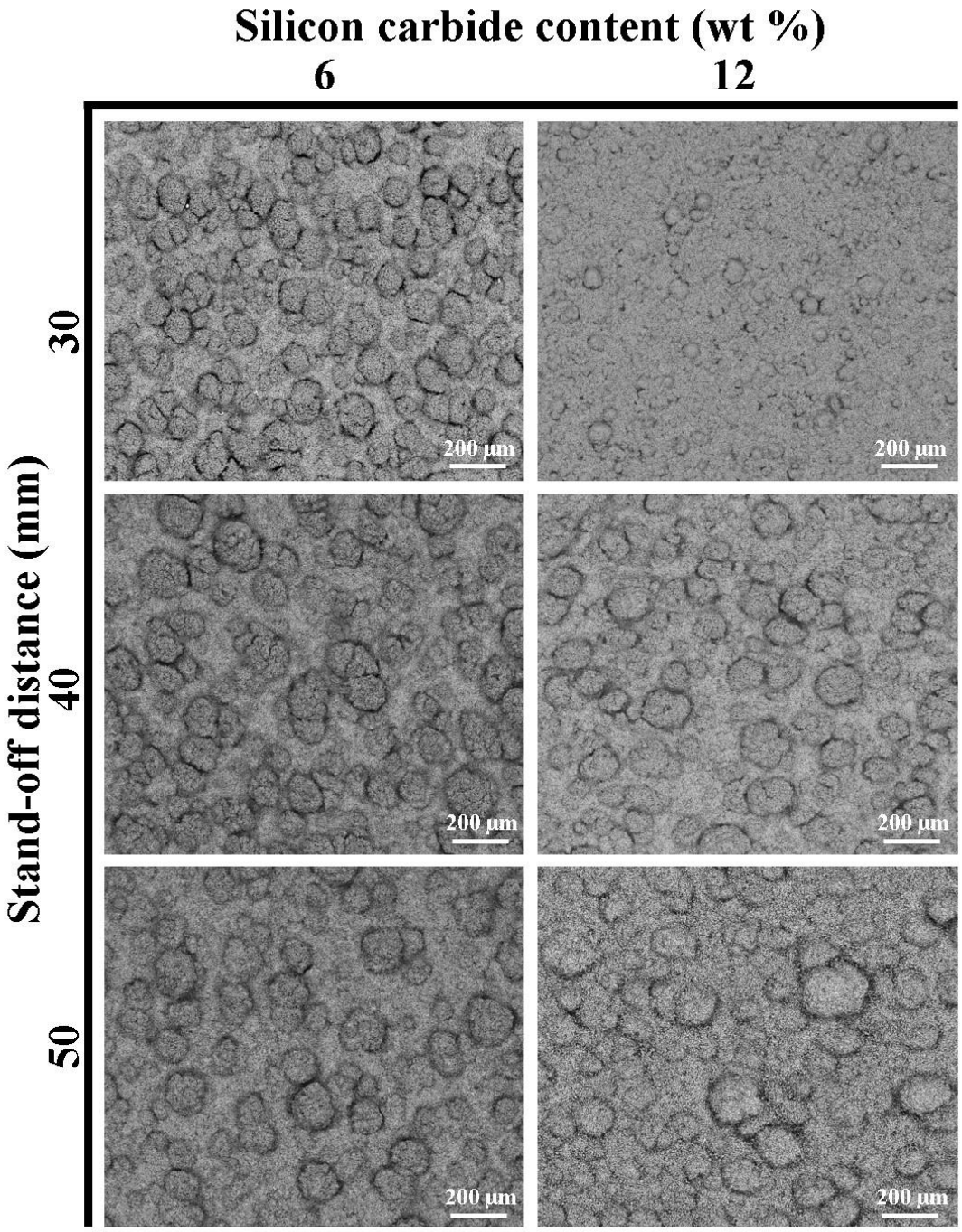

Fig. 3 Surface micrographs of the coatings obtained from the two suspension feedstocks (6 wt% and 12 wt% SiC) at the three stand-off distances (30, 40, and 50 mm).

With regard to cross-sectional micrographs displayed in Fig. 4a, all coatings present a two-zone microstructure also common in SPS coatings [35,36]. These two zones

correspond to the dense zone formed from fully molten particles (marked FM in Fig. 4b micrograph), and the agglomerated zone (partially molten) formed from solid particles that arrive on the substrate in a solid state (marked PM in Fig. 4b micrograph). The reason for this microstructure relates to the fact that a high amount of plasma power is used to evaporate the liquid, resulting in particles or agglomerates, which were just partially molten and then embedded by the fully molten solid. Overall, on observing the six micrographs in Fig. 4a no great differences in terms of the two-zones microstructure are appreciated. Finally, the columnar-like microstructure is not well developed in any of the obtained coatings in contrast with results reported in the literature because the relatively thin layers of the obtained coatings (lower than 80 μm) do not allow a plenty columnar growth to occur. With regard to coating thickness, no significant differences were observed among the different coatings and stand-off distances since feedstock concentration and amount of torch scans were the same for all the experiments.

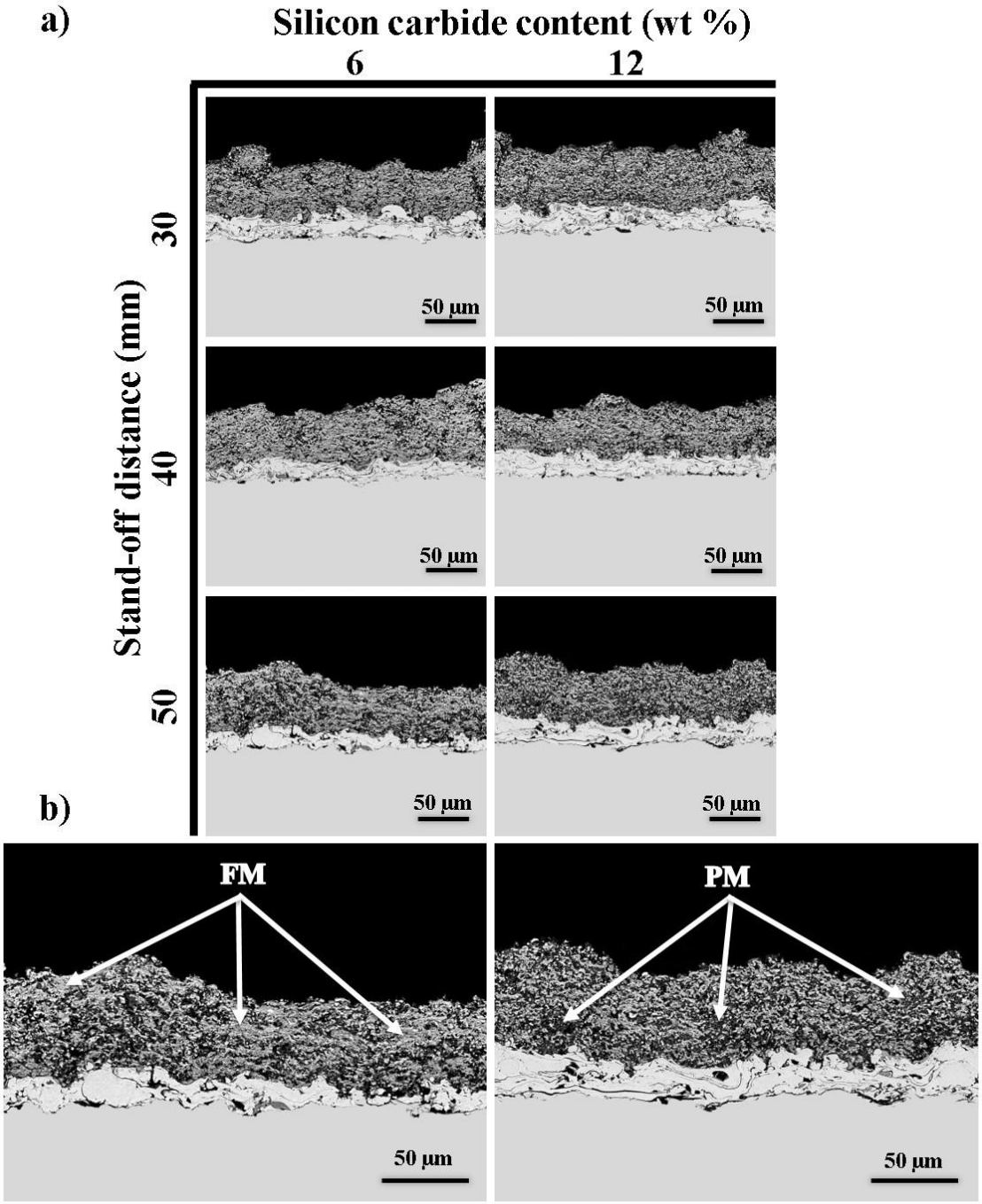

Fig. 4. a) Cross-sectional micrographs of the coatings obtained from the two suspension feedstocks (6 wt% and 12 wt%) at the three stand-off distances (30, 40 and 50 mm). b) Detail of the area in the microstructure of the coatings (melted and partially melted areas).

Porosity of all the coatings was determined by image analysis coupled to the scanning electron microscope. Fig. 5 shows the porosity results. As it can be seen porosity values vary significantly between 8 to 25% as a consequence of the great variations in stand-off distances tested. Furthermore, for the two types of feedstocks, minimum porosity values were found for the intermedium stand-off distance of 40 mm, while the amount of SiC particles in the feedstock suspension does not seem to have a clear effect on porosity. These values are quite consistent with previous findings obtained with SPS coatings of alumina-zirconia suspensions (without SiC particles) as reported by Carpio et al. [24] who highlighted the effect of spraying distance on coating properties by using the same plasma torch. The optimum distance for minimizing porosity is found when the liquid evaporates and the solid melts but the resolidification is avoided. This balance is also affected by solid concentration in the feedstock. Thus, these authors reported an optimum distance of 40 mm in the case of coatings obtained from 10 and 15 vol.% alumina-zirconia SPS suspensions.

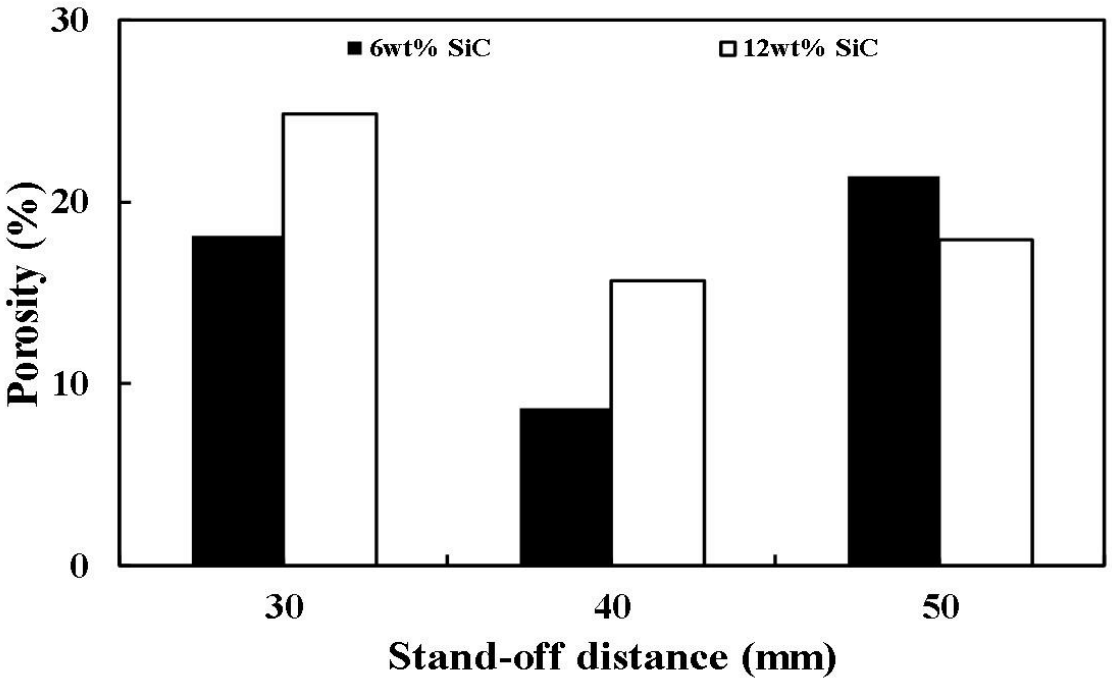

Fig. 5 Porosity values of the coatings obtained from the two suspension feedstocks (6 wt% and 12 wt% SiC) at the three stand-off distances (30, 40, and 50 mm).

3.3. Assessment of preserved SiC particles in the coatings

Fig. 6 shows the XRD patterns of both coatings (6 wt% and 12 wt% SiC) obtained at the intermediate 40 mm stand-off distance, together with the pattern of the powder sample collected from the 12 wt% SiC SPS feedstock. Similar diffractogram profiles were obtained for the other coatings. As observed, the two coatings display practically identical XRD patterns, including almost the same zirconia and alumina peaks, i.e tetragonal Y-TZP and α-alumina. Also, a small α-silicon carbide peak can be distinguished, while peaks or phases of silica are not present. Besides, patterns resemble in large extent the corresponding spectrum of the initial powder with the only difference that the initial powder shows the peaks of baddeleyite (monoclinic zirconia) contained in the zirconia powder (see Table 1) which practically disappears after the plasma spraying process. In all the cases, the appreciation of this SiC peak is not easy since it is quite overlapped with

alumina and zirconia peaks [37,38]. Nevertheless, the SiC peak is a little bit more visible as the SiC content in the coating sample increases (12 wt% against 6 wt%). This finding indicates that, in principle, a measurable amount of the initial SiC has not been either oxidised or decomposed during the plasma deposition.

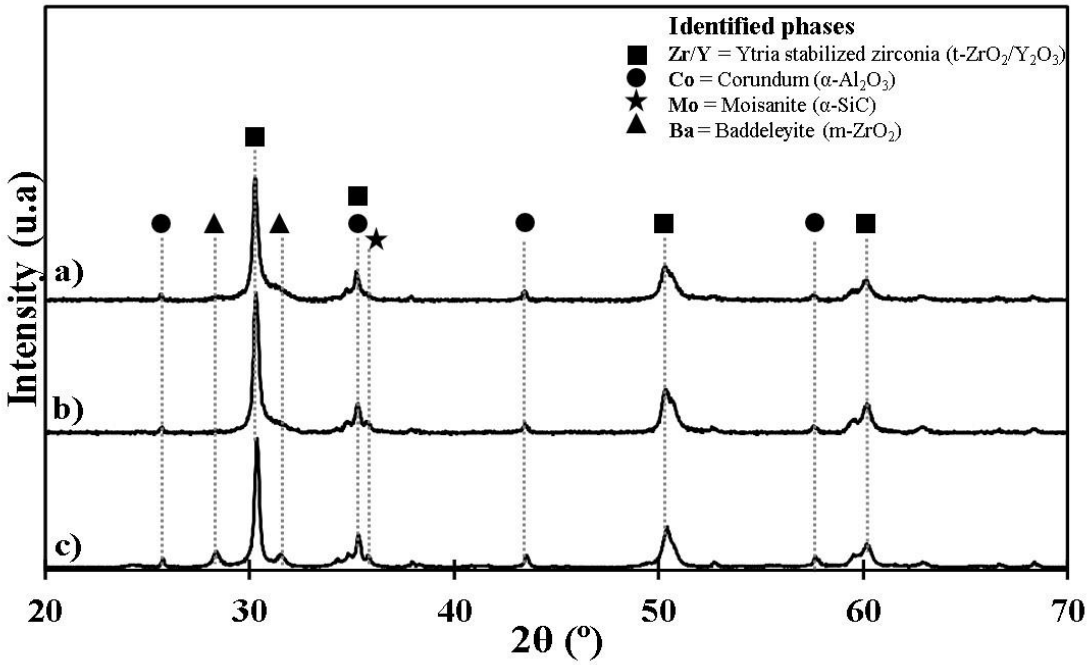

Fig. 6 XRD patterns of the coatings obtained from the two suspension feedstocks a) 6 wt% SiC and b) 12 wt% SiC, at the intermedium stand-off distance of 40 mm, together with the spectrum of the powder sample contained in the 12 wt% SiC suspension feedstock (c).

Fig. 7 shows a higher magnification micrograph of the coating obtained from the 12 wt% SiC feedstock at 40 mm stand-off distance. The micrograph shows the presence of black zones with interconnected pores (marked B in the micrograph) and molten areas of greyish coloration characterised by rounded edges (marked G in the micrographs). This grey-coloured, molten matrix corresponds to the pseudo eutectic mixture of zirconia and alumina which is distributed throughout the coating [21,36]. Lighter or darker greyish zones refer to higher or lower amount or zirconia particles. More interestingly,

micrograph also shows the presence of isolated particles with high silicon contents, characterised by an angular or subangular morphology (marked S). These particles are assumed to correspond to silicon carbide as deduced by EDX analysis also displayed in Fig. 7.

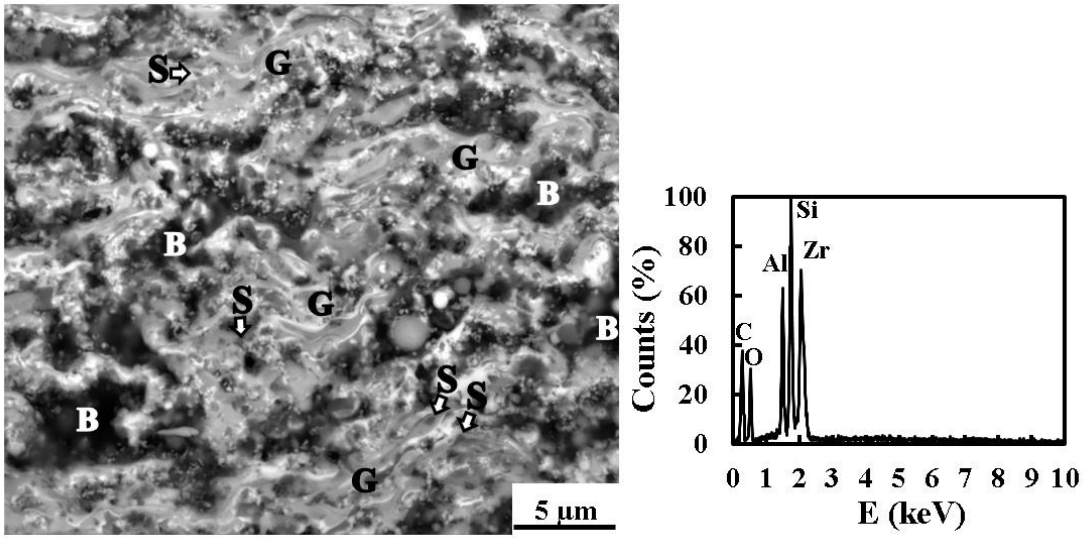

Fig. 7 Higher magnification micrograph of the coating obtained from the 12 wt% SiC feedstock at 40 mm stand-off distance. EDX analysis of S particles is also displayed.

A further identification of the presence of SiC particles in the final coating was carried out by thermogravimetric (TG) analysis. Thus, powder samples of the 12 wt% SiC feedstock before and after being fed into the plasma torch were analysed together with a sample of the used SiC powder. Fig. 8 shows the three plots obtained. As observed, the two powder samples undergo similar weight gain as the reference sample of SiC corresponding to the oxidation of SiC particles starting at 900 °C (marked arrows in the plots) as reported elsewhere [38]. As the test finishes at 1200 °C, no further weight change over this temperature can be observed. Although quantitative assessment is not feasible, Fig. 8 also shows that weight gain in the powder sample after plasma torch is

approximately half of that of the same powder before plasma treatment (0.04% against 0.08%). These findings confirm the preservation of a significant amount of the initial SiC particles in the final coatings.

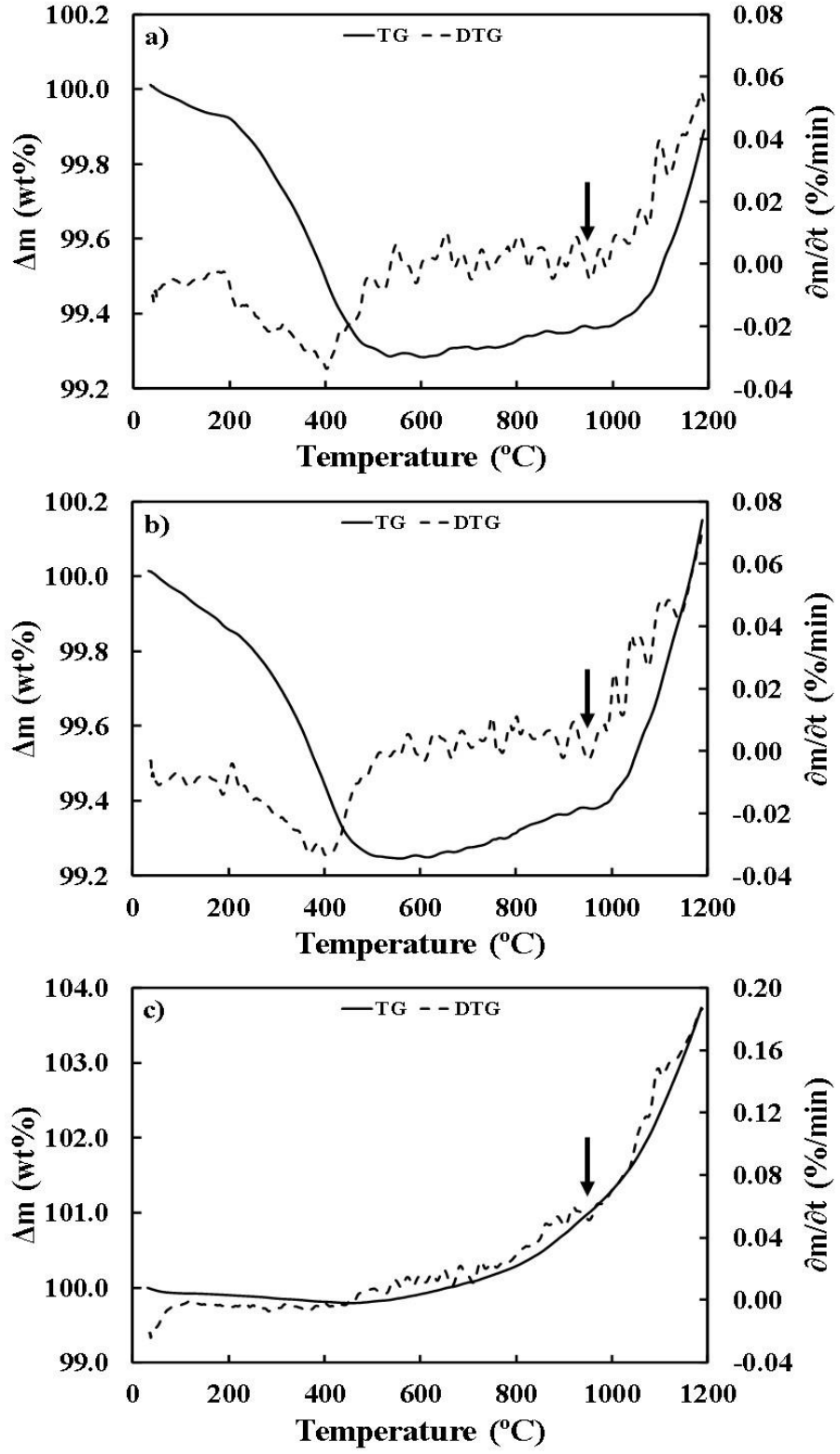

Fig. 8 TG-DTG plots of powder samples of a) 12 wt% SiC coatings and b) 12 wt% SiC feedstock together with a sample of the used c) SiC powder. Arrows refer to the beginning of SiC particles oxidation.

In an attempt to quantify the amount of the preserved SiC in the final coatings, a powder sample collected from both feedstocks (6 wt% and 12 wt% SiC) after being fed into the plasma torch together with the solid contained in these same suspension feedstocks before being plasma sprayed were analysed by XRD technique as set out above. As an example, Fig. 9 shows the XRD patterns obtained for 12 wt% SiC feedstock powders for diffraction angles ranging from 33° to 37°. In this figure peaks have been identified as set out in previous Fig. 6. Due to the overlapping of peaks, this analysis is only relevant for peak 1 (t-ZrO_2) and 2 (alpha SiC). From this analysis, Table 2 has been made in which the quantification of the material preserve in the coatings (referred as % residual) by means of two peaks has been carried out for the two feedstocks (6 wt% and 12 wt%). Data in this table show that while around ~~65%~~ 35% of zirconia matrix melts during plasma spraying, almost 80% of the initial SiC particles is preserved in the final coatings for both feedstocks.

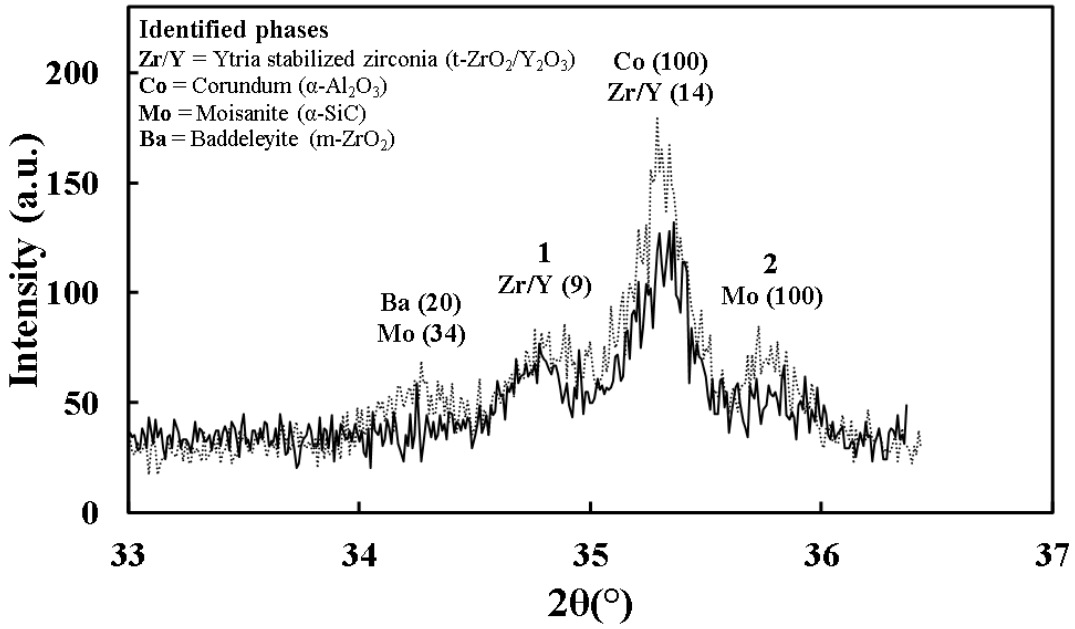

Fig. 9 XRD pattern obtained from powder sample of 12 wt% SiC feedstock suspensions before (dotted line) and after (continuous line) being plasma sprayed for peak area analysis (as set out in section 2.3).

Table 2 Quantification of the peak areas (peaks 1 and 2) of the crystalline phases as set out in Figure 9.

Peaks area						
Peak	**S/A/Z Powder at 10 vol.% slurry with 6 wt% SiC**			**S/A/Z Powder at 10 vol.% slurry with 12 wt% SiC**		
	Area (after plasma)	Area (before plasma)	% residual (*)	Area (after plasma)	Area (before plasma)	% residual (*)
1	28.9	18.6	64.3	22.2	14.5	65.3
2	16.1	12.4	77.0	18.5	14.9	80.1

(*) (peak area in plasma sprayed powder/ peak area in feedstock)*100

4. Conclusions

In this research two suspensions of a Y-TZP/Al_2O_3 matrix with different SiC particle contents (6 wt% and 12 wt%) were prepared as feedstocks for SPS deposition. Suspensions were prepared and it was observed that in both cases, suspensions presented suitable dispersion degree and stability so as to be fed into the plasma torch by SPS process. Three stand-off distances were tested with both feedstocks.

Cauliflower-like microstructures similar to those described in the literature as typical microstructures for suspension feedstocks were obtained regardless the nature of the feedstock (amount of SiC particles). This type of microstructure intensifies as the stand-off distance increases. A cross-sectional view of the coatings shows the two-zone microstructure also common in SPS coatings, which is made up of fully molten particles and an agglomerated zone formed from solid particles that arrive to the substrate in a solid state. Coatings porosity values vary significantly between 8 to 25% as a consequence of the great variations in stand-off distances tested whereas minimum porosity was found for the intermediate stand-off distance of 40 mm with both feedstocks.

Microstructural analysis reveals the presence of SiC particles in the coatings. This presence is demonstrated through EDX analysis and XRD tests. Further confirmation of SiC particles in the coatings was carried out by TG analysis compared with SiC powder. Finally, quantification of SiC content in the coatings by means of XRD analysis showed that most of SiC particles of the feedstocks (c.a 80 %) were preserved in the final coatings. These findings prove the validity of the strategy of using SPS technique as coating process to preserve SiC particles through an atmospheric plasma spray application.

Acknowledgments

This work has been supported by the Spanish Ministry of Economy, Industry and Competitiveness and European Regional Development Fund trough Grant no. MAT2015-67586-C3-R.

Reference

[1] E. Bakan, R. Vaßen, Ceramic top coats of plasma-sprayed thermal barrier coatings: materials, processes, and properties, J. Therm. Spray Technol. 26 (2017) 992–1010. doi:10.1007/s11666-017-0597-7.

[2] C.U. Hardwicke, Y.C. Lau, Advances in thermal spray coatings for gas turbines and energy generation: A review, J. Therm. Spray Technol. 22 (2013) 564–576. doi:10.1007/s11666-013-9904-0.

[3] D.R. Clarke, M. Oechsner, N.P. Padture, Thermal-barrier coatings for more efficient gas-turbine engines, MRS Bull. 37 (2012) 891–898. doi:10.1557/mrs.2012.232.

[4] B. Bernard, L. Bianchi, A. Malié, A. Joulia, B. Rémy, Columnar suspension plasma sprayed coating microstructural control for thermal barrier coating application, J. Eur. Ceram. Soc. 36 (2016) 1081–1089. doi:10.1016/j.jeurceramsoc.2015.11.018.

[5] A. Ganvir, N. Curry, S. Björklund, N. Markocsan, P. Nylén, Characterization of Microstructure and Thermal Properties of YSZ Coatings obtained by Axial Suspension Plasma Spraying (ASPS), J. Therm. Spray Technol. 24 (2015) 1195–1204. doi:10.1007/s11666-015-0263-x.

[6] B. Bernard, A. Quet, L. Bianchi, A. Joulia, A. Malié, V. Schick, B. Rémy, Thermal insulation properties of YSZ coatings: Suspension Plasma Spraying (SPS) versus Electron Beam Physical Vapor Deposition (EB-PVD) and Atmospheric Plasma Spraying (APS), Surf. Coatings Technol. 318 (2017) 122–128. doi:10.1016/j.surfcoat.2016.06.010.

[7] W. Fan, Y. Bai, Review of suspension and solution precursor plasma sprayed thermal barrier coatings, Ceram. Int. 42 (2016) 14299–14312. doi:10.1016/j.ceramint.2016.06.063.

[8] M.R. Loghman-Estarki, R. Shoja Razavi, H. Jamali, Thermal stability and sintering behavior of plasma sprayed nanostructured 7YSZ, 15YSZ and 5.5SYSZ coatings at elevated temperatures, Ceram. Int. 42 (2016) 14374–14383. doi:10.1016/j.ceramint.2016.05.203.

[9] S. Mahade, N. Curry, S. Björklund, N. Markocsan, P. Nylén, Engineered thermal barrier coatings deposited by suspension plasma spray, Mater. Lett. 209 (2017) 517–521. doi:10.1016/j.matlet.2017.08.096.

[10] R. Vassen, A. Stuke, D. Stöver, Recent developments in the field of thermal barrier coatings, J. Therm. Spray Technol. 18 (2009) 181–186. doi:10.1007/s11666-009-9312-7.

[11] H. Dai, X. Zhong, J. Li, Y. Zhang, J. Meng, X. Cao, Thermal stability of double-ceramic-layer thermal barrier coatings with various coating thickness, Mater. Sci. Eng. A. 433 (2006) 1–7. doi:10.1016/j.msea.2006.04.075.

[12] V. Viswanathan, G. Dwivedi, S. Sampath, Multilayer, multimaterial thermal barrier coating systems: Design, synthesis, and performance assessment, J. Am. Ceram. Soc. 98 (2015) 1769–1777. doi:10.1111/jace.13563.

[13] M. Saremi, Z. Valefi, Thermal and mechanical properties of nano-YSZ-Alumina functionally graded coatings deposited by nano-agglomerated powder plasma spraying, Ceram. Int. 40 (2014) 13453–13459. doi:10.1016/j.ceramint.2014.05.068.

[14] A. Portinha, V. Teixeira, J. Carneiro, J. Martins, M.F. Costa, R. Vassen, D. Stoever, Characterization of thermal barrier coatings with a gradient in porosity, Surf. Coatings Technol. 195 (2005) 245–251. doi:10.1016/j.surfcoat.2004.07.094.

[15] S.K. Ghosh, Self-healing materials : fundamentals, design strategies, and applications, Wiley-VCH, Weinheim, Germany, 2009. doi:10.1002/9783527625376.

[16] T. Ouyang, J. Wu, M. Yasir, T. Zhou, X. Fang, Y. Wang, D. Liu, J. Suo, Effect of TiC self-healing coatings on the cyclic oxidation resistance and lifetime of thermal barrier coatings, J. Alloys Compd. 656 (2016) 992–1003. doi:10.1016/j.jallcom.2015.07.271.

[17] F. Tavangarian, G. Li, Synthesis, characterization and formation mechanism of SiC/spinel nanocomposite, J. Alloys Compd. 598 (2014) 106–112. doi:10.1016/j.jallcom.2014.02.047.

[18] F. Nozahic, D. Monceau, C. Estournès, Thermal cycling and reactivity of a $MoSi_2/ZrO_2$ composite designed for self-healing thermal barrier coatings, Mater. Des. 94 (2016) 444–448. doi:10.1016/j.matdes.2016.01.054.

[19] Z. Derelioglu, A.L. Carabat, G.M. Song, S. van der Zwaag, W.G. Sloof, On the use of B-alloyed $MoSi_2$ particles as crack healing agents in yttria stabilized zirconia thermal barrier coatings, J. Eur. Ceram. Soc. 35 (2015) 4507–4511. doi:10.1016/j.jeurceramsoc.2015.08.035.

[20] T. Ouyang, X. Fang, Y. Zhang, D. Liu, Y. Wang, S. Feng, T. Zhou, S. Cai, J. Suo, Enhancement of high temperature oxidation resistance and spallation resistance of SiC-self-healing thermal barrier coatings, Surf. Coatings Technol. 286 (2016) 365–375. doi:10.1016/j.surfcoat.2015.12.054.

[21] V. Carnicer, C. Alcazar, R. Moreno, E. Sánchez, Aqueous suspension processing of multicomponent submicronic Y-TZP/Al2O3/SiC particles for suspension plasma spraying, J. Eur. Ceram. Soc. (2017). doi:https://doi.org/10.1016/j.jeurceramsoc.2018.01.006.

[22] F. Tarasi, M. Medraj, A. Dolatabadi, J. Oberste-Berghaus, C. Moreau, Effective parameters in axial injection suspension plasma spray process of alumina-zirconia ceramics, J. Therm. Spray Technol. 17 (2008) 685–691. doi:10.1007/s11666-008-9259-0.

[23] R. Garvie, Structural applications of ZrO_2 bearing materials, in: N. et al Claussen (Ed.), Zirconia II., Adv. Ceram., American Ceramic Society, Westerville, Ohio, 1984: pp. 465–478.

[24] P. Carpio, M.D. Salvador, A. Borrell, E. Sánchez, R. Moreno, Alumina-zirconia coatings obtained by suspension plasma spraying from highly concentrated aqueous suspensions, Surf. Coatings Technol. 307 (2016) 713–719. doi:10.1016/j.surfcoat.2016.09.060.

[25] V.M. Candelario, F. Guiberteau, R. Moreno, A.L. Ortiz, Aqueous colloidal processing of submicrometric SiC plus $Y_3Al_5O_{12}$ with diamond nanoparticles, J. Eur. Ceram. Soc. 33 (2013) 2473–2482. doi:10.1016/j.jeurceramsoc.2013.04.016.

[26] E. Cañas, M. Vicent, M.J. Orts, R. Moreno, E. Sánchez, Bioactive glass suspensions preparation for suspension plasma spraying, J. Eur. Ceram. Soc. 36

(2016) 4281–4290. doi:10.1016/j.jeurceramsoc.2016.06.011.

[27] E. Bannier, G. Darut, E. Sánchez, A. Denoirjean, M.C. Bordes, M.D. Salvador, E. Rayón, H. Ageorges, Microstructure and photocatalytic activity of suspension plasma sprayed TiO_2 coatings on steel and glass substrates, Surf. Coatings Technol. 206 (2011) 378–386. doi:10.1016/j.surfcoat.2011.07.039.

[28] P. Carpio, E. Bannier, M.D. Salvador, A. Borrell, R. Moreno, E. Sánchez, Effect of particle size distribution of suspension feedstock on the microstructure and mechanical properties of suspension plasma spraying YSZ coatings, Surf. Coatings Technol. 268 (2015) 293–297. doi:10.1016/j.surfcoat.2014.08.063.

[29] B.D. Cullity, S.R. Stock, Elements of X-ray diffraction, Third Edit, Upper Saddle River, NJ : Prentice-Hall, New York, 2001.

[30] M. Vicent, E. Sánchez, G. Mallol, R. Moreno, Study of colloidal behaviour and rheology of Al_2O_3-TiO_2 nanosuspensions to obtain free-flowing spray-dried granules for atmospheric plasma spraying, Ceram. Int. 39 (2013) 8103–8111. doi:10.1016/j.ceramint.2013.03.083.

[31] O. Mengual, G. Meunier, I. Cayré, K. Puech, P. Snabre, TURBISCAN MA 2000: Multiple light scattering measurement for concentrated emulsion and suspension instability analysis, Talanta. 50 (1999) 445–456. doi:10.1016/S0039-9140(99)00129-0.

[32] P. Fauchais, R. Etchart-Salas, V. Rat, J.F. Coudert, N. Caron, K. Wittmann-Ténèze, Parameters controlling liquid plasma spraying: Solutions, sols, or suspensions, J. Therm. Spray Technol. 17 (2008) 31–59. doi:10.1007/s11666-007-9152-2.

[33] P. Sokolowski, S. Kozerski, L. Pawlowski, A. Ambroziak, The key process

parameters influencing formation of columnar microstructure in suspension plasma sprayed zirconia coatings, Surf. Coatings Technol. 260 (2014) 97–106. doi:10.1016/j.surfcoat.2014.08.078.

[34] L. Latka, S.B. Goryachev, S. Kozerski, L. Pawlowski, Sintering of fine particles in suspension plasma sprayed coatings, Materials (Basel). 3 (2010) 3845–3866. doi:10.3390/ma3073845.

[35] S. Kozerski, L. Łatka, L. Pawlowski, F. Cernuschi, F. Petit, C. Pierlot, H. Podlesak, J.P. Laval, Preliminary study on suspension plasma sprayed ZrO_2+8wt.% Y_2O_3 coatings, J. Eur. Ceram. Soc. 31 (2011) 2089–2098. doi:10.1016/j.jeurceramsoc.2011.05.014.

[36] P. Carpio, A. Borrell, M.D. Salvador, A. Gómez, E. Martínez, E. Sánchez, Microstructure and mechanical properties of plasma spraying coatings from YSZ feedstocks comprising nano- and submicron-sized particles, Ceram. Int. 41 (2015) 4108–4117. doi:10.1016/j.ceramint.2014.11.106.

[37] Z. Károly, C. Bartha, I. Mohai, C. Balázsi, I.E. Sajõ, J. Szépvölgyi, Deposition of silicon carbide and nitride-based coatings by atmospheric plasma spraying, Int. J. Appl. Ceram. Technol. 10 (2013) 72–78. doi:10.1111/j.1744-7402.2011.02748.x.

[38] Y. Lin, L. Chen, Oxidation of SiC powders in SiC/alumina/zirconia compacts, Ceram. Int. 26 (2000) 593–598. doi:10.1016/S0272-8842(99)00102-9.